Atmospheric
Chemistry
and Physics

Aerosol physicochemical properties and implications for visibility during an intense haze episode during winter in Beijing

Y. H. Wang[1,2], Z. R. Liu[1], J. K. Zhang[1], B. Hu[1], D. S. Ji[1], Y. C. Yu[1], and Y. S. Wang[1,2]

[1]State Key Laboratory of Atmospheric Boundary Layer Physics and Atmospheric Chemistry (LAPC), Institute of Atmospheric Physics, Chinese Academy of Sciences, Beijing, 100029, China
[2]College of Atmospheric Sciences, Lanzhou University, Lanzhou, 730000, China

Correspondence to: Y. S. Wang (wys@mail.iap.ac.cn)

Abstract. The evolution of physical, chemical and optical properties of urban aerosol particles was characterized during an extreme haze episode in Beijing, PRC, from 24 through 31 January 2013 based on in situ measurements. The average mass concentrations of PM_1, $PM_{2.5}$ and PM_{10} were $99 \pm 67\,\mu g\,m^{-3}$ (average $\pm$ SD), $188 \pm 128\,\mu g\,m^{-3}$ and $265 \pm 157\,\mu g\,m^{-3}$, respectively. A significant increase in $PM_{1-2.5}$ fraction was observed during the most heavily polluted period. The average scattering coefficient at 550 nm was $877 \pm 624\,Mm^{-1}$. An increasing relative amount of coarse particles can be deduced from the variations of backscattering ratios, asymmetry parameter and scattering Ångström exponent. Particle number-size distributions between 14 and 2500 nm diameter showed high number concentrations, particularly in the nucleation mode and accumulation mode. Size-resolved chemical composition of submicron aerosol from a high-resolution time-of-flight aerosol mass spectrometer showed that the mass concentrations of organic, sulfate, nitrate, ammonium and chlorine mainly resided on particles between 500 and 800 nm (vacuum diameter), and nitrate and ammonium contributed greatly to particle growth during the heavily polluted day (28 January).

Increasing relative humidity and stable synoptic conditions on 28 January combined with heavy pollution on 28 January, leading to enhanced water uptake by the hygroscopic submicron particles and formation of secondary aerosol, which might be the main reasons for the severity of the haze episode. Light-scattering apportionment showed that organic, sulfate, ammonium nitrate and ammonium chloride compounds contributed to light-scattering fractions of 54, 24, 12 and 10 %, respectively. This study indicated that the organic component in submicron aerosol played an important role in visibility degradation during the haze episode in Beijing.

1 Introduction

Atmospheric aerosol particles play a significant role in radiation balance and climate forcing through direct scattering and absorption of solar radiation (Anderson et al., 2003; Pöschl, 2005; Ramanathan et al., 2001). In addition, they can act as cloud condensation nuclei (CCN) and thereby change the cloud albedo and lifetime (Twomey, 1977). Accordingly, the radiative properties of clouds are indirectly influenced by aerosol (Kaufman et al., 2005; Koren et al., 2005; Lohmann and Feichter, 2005). Furthermore, the general public has to pay special attention to atmospheric aerosol due to its deleterious effect on human health and degradation of visibility (Nel, 2005; Watson, 2002), which are closely related to the chemical components, morphology, mixing state, size distribution and hygroscopic properties of aerosol particles.

Along with the rapid economic growth in China, its capital city, Beijing, has suffered substantially from air quality deterioration and visibility degradation, though the mass concentration of PM_{10} has decreased in Beijing in the last 10 years (Liu et al., 2015). Accompanied by frequent fog-haze days, the visibility in Beijing has decreased dramatically to an unacceptable level. The frequency of visibility between 2 and 10 km has increased from 37 % in 1999 to 43 % in 2007. (Zhang et al., 2010; Zhang et al., 2012). The mass loading of fine aerosol particles and their precursors (e.g., NH_3, volatile

organic compounds (VOCs), SO$_2$ and NO$_x$) can accumulate to high levels within the planetary boundary layer , especially during periods of persistent synoptic-scale stagnation and strong temperature inversions (Zhang et al., 2013). In the past decade, many research projects have been undertaken to characterize the chemical and physical properties of aerosol particles in Beijing and its surrounding regions. These studies mainly focused on the following aspects:

i. chemical composition, evaluation and sources apportionment based on filter sampling and aerosol mass spectrometry (AMS) (Huang et al., 2010b; Sun et al., 2006; Zhang et al., 2014);

ii. mass concentration and optical properties of aerosol particles using in situ measurements or combined with MODIS (Moderate-Resolution Imaging Spectroradiometer) satellite remote sensing optical depth products (He et al., 2009; Huang et al., 2010a; Li et al., 2010; Qu et al., 2010; Wang, K. C. et al., 2012; Yang et al., 2009);

iii. aerosol hygroscopic properties, number-size distributions, mixing state and implications for CCN activity, visibility, new particle formation, air pollution and radiative forcing (Chen et al., 2012; Cheng et al., 2012; Deng et al., 2013; Liu et al., 2013; Ma et al., 2012; Meier et al., 2009; Pan et al., 2009; Quan et al., 2011; Wehner et al., 2008; Wu et al., 2007; Zhang et al., 2010; Zhang et al., 2011).

The abovementioned studies, based on either long-term or short-term observations, provide us with comprehensive knowledge of aerosol properties on days with near-average aerosol concentration levels. However, only a few studies have been carried out on highly polluted days, and these studies mainly focus on variations of chemical composition with the evaluation of synoptic conditions and planetary boundary layer dynamics (Huang et al., 2010a; Wang, L. et al., 2012; Zhao et al., 2013). The interaction between chemical and physical properties of aerosols has seldom been investigated during haze episodes. Therefore, comprehensive studies of physical, optical and chemical properties using high-resolution measurements are necessary for a better knowledge of aerosol evolution processes and related visibility degradation during pollution episodes in Beijing.

An intense pollution episode occurred in central and eastern China from 24 through 31 January 2013. The hourly average PM$_{10}$ exceeded 600 μg m^{-3}, and non-refractory submicron particles (NR-PM$_1$) exceeded 400 μg m^{-3} (Wang et al., 2013), which was the most extreme haze episode in Beijing in the last decades as far as we know. In this study, we investigated the evolution of physical, chemical and optical properties of urban aerosol particles during the haze episode by using the in situ measurements.
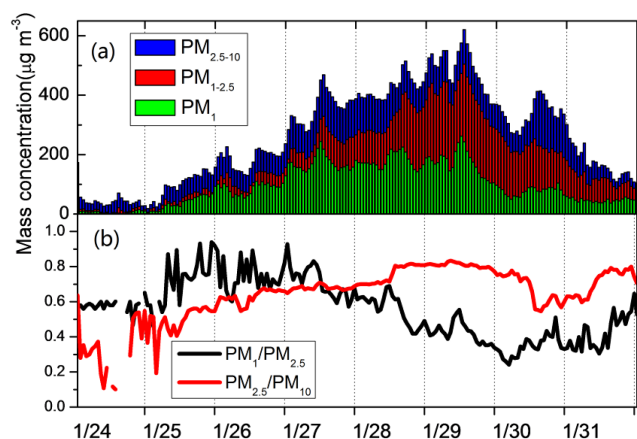
2　Methodology

Site information and instrumentation

The aerosol sampling site was situated on the roof (about 15 m above the surface) of a laboratory building in the yard of the Institute of Atmospheric Physics (IAP), Chinese Academy of Sciences, which was located between the third and fourth ring roads of northeast Beijing (Zhang et al., 2014).

An integrating nephelometer (Model 3563, TSI Inc., Minnesota, USA) was used to measure the total light-scattering and hemispheric backscattering coefficients (for angles of 7 to 170° and 90 to 170°, respectively) of low-relative-humidity (RH) aerosol at wavelengths of 450, 550 and 700 nm; no size-selective inlets were used. The nephelometer was operated at 5 L min^{-1} with data resolution of 1 min. A calibration was conducted every month with filtered air and CO$_2$ as prescribed by the manufacturer. Subsequently, the data were corrected for truncation errors and the non-lambertian light source based on the measured Ångström exponents (Anderson and Ogren, 1998). On average, the corrected values were within 10 % of the measured values. The mass concentration of PM$_{10}$ and PM$_{2.5}$ were measured by a Thermo TEOM 1400AB/8500 FDMS (Filter Dynamic Measurement System). The mass concentration of PM$_1$ was determined using a Thermo TEOM 1400.

The particle number-size distribution between 14 and 2500 nm diameter was measured by a Scanning Mobility Particle Sizer (SMPS, TSI Inc., Minnesota, USA), comprised of a model TSI 3080 Electrostatic Classifier and a model TSI 3775 Condensation Particle Counter (CPC), and an Aerodynamic Particle Sizer (APS, Model 3321, TSI Inc., Minnesota, USA). The SMPS data covered the particle size range from 14 to 533 nm, and the APS covered the range from 542 to 2500 nm. The size-dependent diffusional and gravitational losses for the inlet line have been corrected by using the empirical functions given by Willeke and Baron (1993). The data collected from these two instruments were merged into one particle size spectrum matrix (14 to 2500 nm) according to the methods of Liu et al. (2014) and Beddows et al. (2010).

The aerosol chemical composition was acquired using an Aerodyne High-Resolution Time-of-Flight Aerosol Mass Spectrometer (HR-ToF-AMS, or AMS, Aerodyne Research Inc., Billerica, MA, USA). The organic matter, sulfate, nitrate, ammonium and chlorine in non-refractory submicron particle mass-size distributions (NR-PM$_1$) were determined under V and W ion optical modes alternatively every 7.5 min. Detailed information of data analysis, collection efficiency (CE) and relative ionization efficiency of the instrument were introduced by Zhang et al. (2014). Simultaneously, the gaseous pollutants (e.g., NO, NO$_x$, CO, O$_3$ and SO$_2$) were measured using Thermo instruments (series of 42i, 48i, 49i and 43i, respectively; Thermo Fisher Scientific, Franklin, Massachusetts, USA). Detailed introduction and calibrations were given by Tang et al. (2012) and Wang et al. (2014).
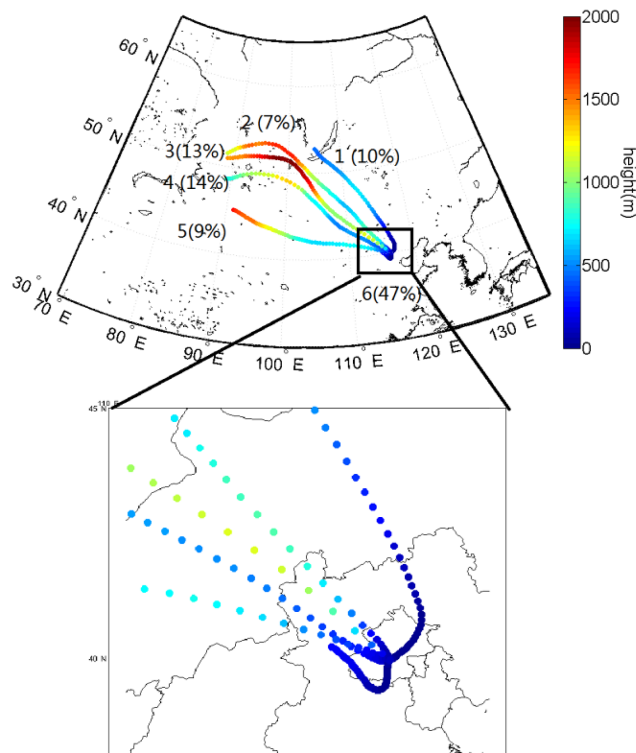
Figure 1. Time series of (a) mass concentrations of PM_1, $PM_{1-2.5}$ and $PM_{2.5-10}$; (b) mass ratios of $PM_1 / PM_{2.5}$ and $PM_{2.5} / PM_{10}$.

An automatic meteorological observation instrument (Milos520, Vaisala, Finland) was used to obtain meteorological parameters (relative humidity, air temperature, wind speed and direction). The time base for all data in the study was Beijing zone time (UTC +8).

3 Results and discussion

3.1 Aerosol mass concentration and meteorological parameters

Figure 1 shows the mass concentrations of PM_1, $PM_{1-2.5}$, $PM_{2.5-10}$ and mass concentration ratios of $PM_1 / PM_{2.5}$ and $PM_{2.5} / PM_{10}$ during the period. The average mass concentrations of PM_1, $PM_{2.5}$ and PM_{10} are 99.1 ± 67.1, 188.3 ± 128.8 and $265.2 \pm 157.1\,\mu g\,m^{-3}$, respectively, indicative of the high level of aerosol pollution. The average mass ratios of $PM_1 / PM_{2.5}$ and $PM_{2.5} / PM_{10}$ are 0.56 ± 0.16 and 0.64 ± 0.15, respectively. As we can see in Fig. 1b, the mass ratio of $PM_1 / PM_{2.5}$ is higher than that of $PM_{2.5} / PM_{10}$ before 28 January, indicating that PM_1 dominated the total mass. The aerosol concentration increased gradually and reached the maximum values at 12:00 on 29 January, with PM_1, $PM_{2.5}$ and PM_{10} values of 243.1, 504.6 and $620.8\,\mu g\,m^{-3}$, respectively. The detailed interpretations of the high values will be presented in the following section. Thereafter, the aerosol concentrations decreased rapidly to a lower level. The mass ratios of $PM_1 / PM_{2.5}$ and $PM_{2.5} / PM_{10}$ showed the opposite pattern with time variation during the period, indicating a decreasing fraction of PM_1 compared with $PM_{2.5}$ and an increasing fraction of $PM_{2.5}$ compared with PM_{10} with increasing aerosol pollution. It is worth noting that the increase of $PM_{1-2.5}$ was greatest during the period 28 to 29 January, as shown in Fig. 1a. Figure S1 in the Supplement displays meteorological parameters during the episode. During this period, the average wind speed was $2.5\,m\,s^{-1}$. Figure S2 shows an overview

Figure 2. The 3-day backward trajectory of air parcels during the observation period; the colors of air trajectories represent height during transport.

of the wind rose of the local wind; the wind is mainly in the southerly and northerly quadrant, which can bring relative dirty or clean air masses, respectively. Figure 2 exhibits 72 h backward trajectories of air parcels every 3 h using HYSPLIT model from a height of 100 m, with a total of six clusters yielded (http://ready.arl.noaa.gov/HYSPLIT.php). We should clarify that the southern area of Beijing often suffers a more polluted atmosphere than that in the northern area due to more cities and population. The clusters of 1 to 5 are from the northerly direction, with clean air and high transport height. Furthermore, a long transport pathway within 72 h implies that those air parcels have a higher transport speed compared with cluster 6. Cluster 6, from southern and local directions with a fraction of 47 %, has the highest frequency. The cluster has a short transport distance of nearly 400 km, and low transport height and speed, resulting in a sufficient loading of surface air pollution compared with other clusters. We also present sounding data in Beijing from the University of Wyoming twice a day (http://weather.uwyo.edu/upperair/), as shown in Fig. 3. These lines with different colors represent soundings during the observation period. It is worth noting that an inversion layer between 1000 and 1500 m exists after 27 January. Particularly at 08:00 on 28 January (Beijing time), the lapse rate of temperature is nearly $0.6\,°C\,100\,m^{-1}$, which indicates

Table 1. The statistic of aerosol optical properties during the observation period.

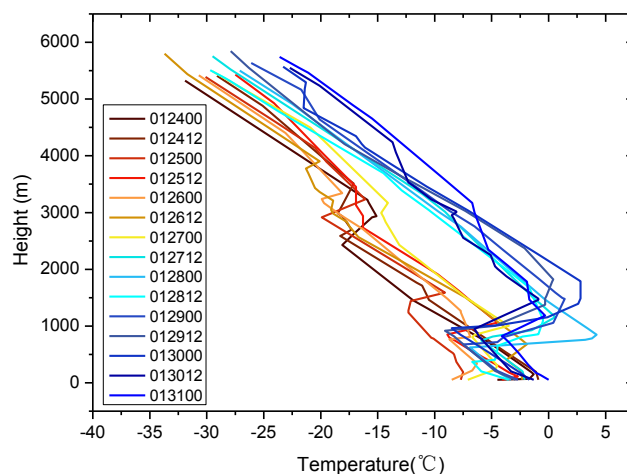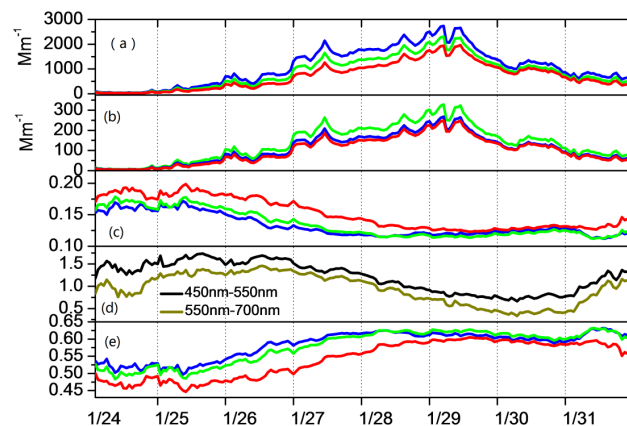| Parameter	Mean	Median	Standard derivation	5 % quantile	95 % quantile
$\sigma_{sp}^{450}(Mm^{-1})$	1088.5	924.4	748.1	48.1	2386.3
$\sigma_{sp}^{550}(Mm^{-1})$	877.2	748.4	624.2	36.6	1993.4
$\sigma_{sp}^{700}(Mm^{-1})$	718.4	628.2	530.9	28.7	1703.3
$\sigma_{bsp}^{450}(Mm^{-1})$	134.4	122.8	87.1	7.6	281.4
$\sigma_{bsp}^{550}(Mm^{-1})$	108.1	96.4	71	6.1	228.5
$\sigma_{bsp}^{700}(Mm^{-1})$	98.7	89.3	66.5	7.3	214.4
b_{450}	0.13	0.13	0.02	0.11	0.16
b_{550}	0.14	0.12	0.02	0.11	0.17
b_{700}	0.15	0.14	0.02	0.13	0.19
$Å_{450/550}$	1.2	1.3	0.3	0.74	1.7
$Å_{550/700}$	0.94	1.0	0.3	0.41	1.4
g_{450}	0.58	0.6	0.04	0.52	0.62
g_{550}	0.57	0.6	0.05	0.50	0.63
g_{700}	0.54	0.56	0.05	0.46	0.60

a very stable synoptic condition. Combined with low wind speed, as shown in Fig. S1, the horizontal motion is also limited during the pollution episode.

3.2 Aerosol optical properties

The aerosol scattering coefficient (σ_{sp}) and backscattering coefficient (σ_{bsp}) can be directly measured by the nephelometer and then aerosol backscattering fraction (b_λ), scattering Ångström exponent ($Å_{sp}$) and asymmetry parameter (g_λ) can be calculated from the scattering coefficients, which have rarely been reported in Beijing using in situ measurements. The aerosol light-scattering coefficients show the same pattern as mass concentration of PM, as shown in Fig. 4. Table 1 shows the statistics of the aerosol optical properties during this haze episode, and the average aerosol scattering coefficients σ_{sp}^{450}, σ_{sp}^{550} and σ_{sp}^{700} are $1088.5 \pm 748.1\,Mm^{-1}$, $877.2 \pm 624.2\,Mm^{-1}$ and $718.4 \pm 530.8\,Mm^{-1}$, respectively. After converting the aerosol light-scattering coefficients at 550 nm to that of 525 nm, the average σ_{sp} at 525 nm are 3.2 times greater than the yearly average values at another site in Beijing, reported by He et al. (2009). The average aerosol backscattering coefficients σ_{bsp}^{450}, σ_{bsp}^{550} and σ_{bsp}^{700} are $134.4 \pm 87.1\,Mm^{-1}$, $108.1 \pm 71.1\,Mm^{-1}$ and $98.7 \pm 66.5\,Mm^{-1}$, respectively, as presented in Fig. 4b. During the whole campaign, σ_{sp} and σ_{bsp} at three wavelengths were highly correlated. Both σ_{sp} and σ_{bsp} increase gradually from 24 to 29 January and decrease sharply to lower levels, which are consistent with the variations of aerosol mass concentrations.
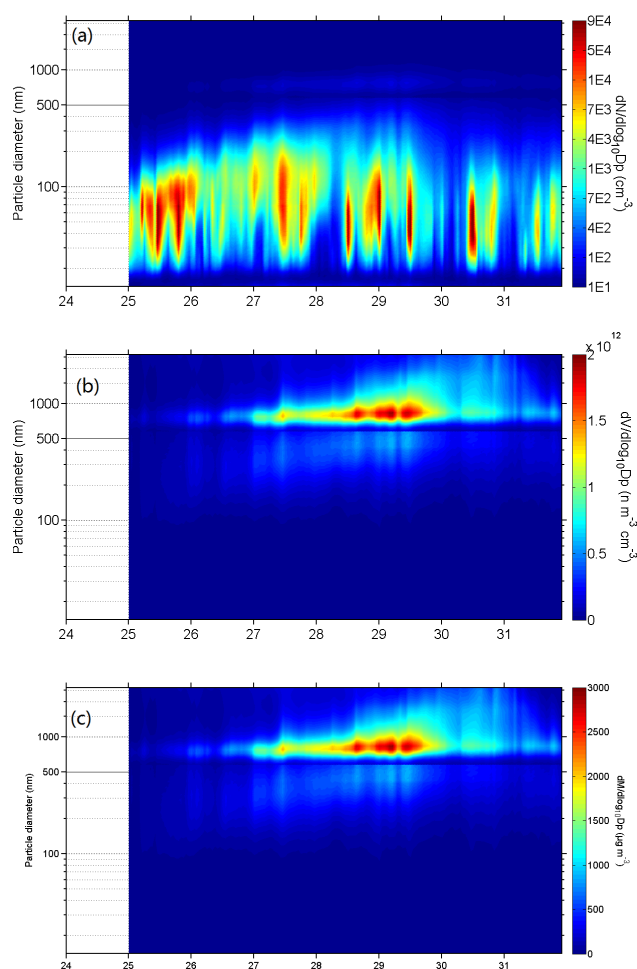
The backscattering ratio, which is also called the hemispheric backscatter fraction, is the ratio of light scattered in the backward hemisphere to the total light scattered by parti-

Figure 3. The temperature profiles during the observation period. The legend stands for UTC time. For example, 012400 means 00:00 on 24 January.

Figure 4. Time series of **(a)** scattering coefficients σ_{sp}, **(b)** backscattering coefficients σ_{bsp}, **(c)** backscattering ratios b_λ, **(e)** asymmetry parameter g_λ at wavelengths of 450 nm (blue), 550 nm (green) and 700 nm (red) **(d)** scattering Ångström exponent ($Å_{sp}$) from 450–550 nm (black) and 550–700 nm (brown).

cles. It is related to particle size distribution and can be calculated as follows:

$$b_\lambda = \frac{\sigma_{bsp}^\lambda}{\sigma_{sp}^\lambda}. \tag{1}$$

The average b_λ at three wavelengths are 0.13 ± 0.02, 0.14 ± 0.02 and 0.15 ± 0.02, respectively. A higher value of b_λ at 700 nm indicates relatively more small size particles that scatter light in the backward hemisphere. The scattering Ångström exponent ($Å_{sp}$) represents the wavelength dependence of scattering coefficient and is related to the slope of the number-size distribution or the mean size and relative concentrations of the accumulation and coarse-mode aerosol.

Figure 5. Time series of **(a)** particle number-size distribution, **(b)** particle volume size distribution, **(c)** particle mass-size distribution between 14.1 and 2458 nm using SMPS combined with APS from 25 to 31 January. The x axis represents the data of January, and the y axis represents particle diameter (nm). The color in panels **(a–c)** represents particle concentration (dN/dlog D_p).

It is calculated using any two of three channels as follows:

$$\mathring{A} = -\frac{\log(\sigma_{sp}^{\lambda_1}) - \log(\sigma_{sp}^{\lambda_2})}{\log(\lambda_1) - \log(\lambda_2)}. \qquad (2)$$

The average $\mathring{A}_{450/550}$ and $\mathring{A}_{550/700}$ are 1.2 ± 0.3 and 0.94 ± 0.3, respectively. The average $\mathring{A}_{450/700}$ is 1.1 ± 0.3, which is smaller than that of 1.46 in Guangzhou (Garland et al., 2008) and 1.7 in Spain reported by Titos et al. (2012), which indicates a more dominant coarse-mode particle compared with the other locations.

The asymmetry parameter g is a fundamental parameter for radiative transfer calculation and is defined as the

intensity-weighted averaged cosine of the scattering angle:

$$g_\lambda = \frac{1}{2} \int_0^\pi \cos\theta \, P(\theta) \sin\theta d\theta, \qquad (3)$$

where θ is the angle between incident light and scattering direction and $P(\theta)$ is the angular distribution of scattered light (the phase function). The value of g_λ ranges from -1 for completely backscattered light to $+1$ for completely forward-scattered light. Because there is no measurement method that can directly obtain the values of g, a fit equation applied by Andrews et al. (2006) was used as in Eq. (4).
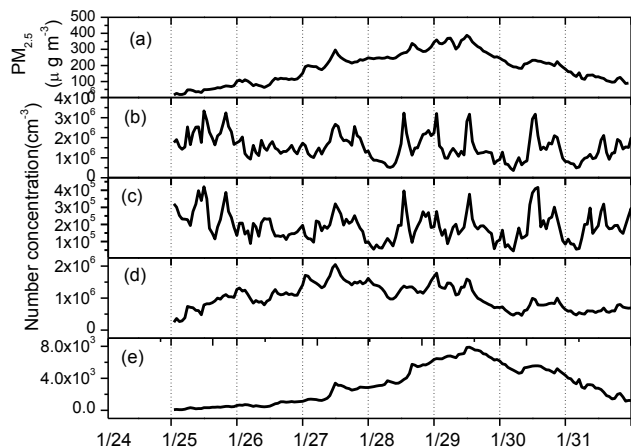
$$g_\lambda = -7.143889 \cdot b_\lambda^3 + 7.464439 \cdot b_\lambda^2 - 3.9356 \cdot b_\lambda + 0.9893 \quad (4)$$

The average value of g_λ at 450, 550 and 700 nm is 0.58 ± 0.04, 0.59 ± 0.05 and 0.54 ± 0.05, respectively. The three parameters of b_λ, $\mathring{A}_{sp}$ and g_λ can show a relative contribution of particle size to light scattering. During 24 and 25 January, b_λ and $\mathring{A}_{sp}$ show higher values, which shows lower ones, as shown in Fig. 4. However, the opposite feature occurs when the haze develops. Especially during the highest pollution periods (from 28 to 30 January), higher values of b_λ and $\mathring{A}_{sp}$, and lower values of g_λ appear, which indicates an increasing fraction of relatively coarse aerosol, consistent with the variation pattern of $PM_1 / PM_{2.5}$ shown in Fig. 1b.

3.3 Particle number-size distribution

The particle number-size distribution from 25 to 31 January is shown in Fig. 5a. The particle number concentration peaks at a diameter of around 100 nm. These particles are mainly from direct emissions of vehicles, cooking and new particle formation (Shi et al., 2001). Particle volume concentration and mass concentration are shown in Fig. 5b and c, respectively, assuming an average aerosol bulk density of $1.5\,\mathrm{g\,cm^{-3}}$ and that all particles are regular spheres based on the research by Zhang et al. (2004) in Pittsburgh, PA, USA. The coarse-mode particles between diameters of 1000 and 2500 nm increased significantly during the most heavily pollution periods (28 and 29 January), as shown in Fig. 5b and c, which is consistent with interpretations of the variation ratio of $PM_1 / PM_{2.5}$. The time series of calculated mass concentration of $PM_{2.5}$, number concentrations of nucleation mode (14–25 nm), Aitken mode (25–100 nm), accumulation mode (100–1000 nm) and coarse mode (1000–2500 nm) are presented in Fig. 6. The calculated mass concentration of $PM_{2.5}$ matches well with measured values, with R^2 values of 0.97, as shown in Fig. S3. The nucleation mode particles show the highest number concentration during the period, with an average value greater than $1.5 \times 10^6\,\mathrm{cm^{-3}}$, indicating large emission of reactive or low-volatility aerosol precursor gases (e.g., sulfur dioxide and organic vapors). The lowest particle number concentration is in coarse mode ($D_m > 1000$ nm), with an average value of $3.18 \times 10^3\,\mathrm{cm^{-3}}$.
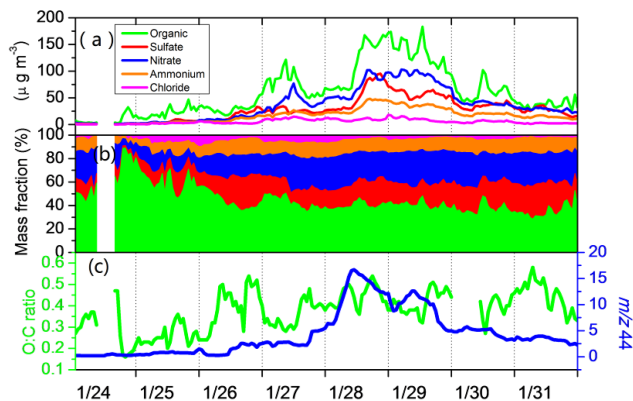
Figure 6. Time series of **(a)** particle mass concentration calculated from number-size distribution and number concentrations of **(b)** nucleation mode (14.1–25 nm), **(c)** Aitken mode (25–100 nm), **(d)** accumulation mode (100–1000 nm) and **(e)** coarse mode (1000–2458 nm) from 25 to 31 January.

Figure 7. Time series of **(a)** mass concentrations of organic, sulfate, nitrate, ammonium and chloride in submicron aerosol; **(b)** mass fractions of organic, sulfate, nitrate, ammonium and chloride; **(c)** O : C ratio and m/z 44 during the haze episode.

The Aitken mode and accumulation mode also show high number concentrations, with average values of 1.90×10^5 and 1.01×10^6 cm^{-3}, respectively. Compared with 3 years of measurements of particle number concentration at another urban site in Beijing, the number concentrations of nucleation, Aitken and accumulation mode during this haze episode are more than 170, 10 and 120 times higher, respectively (Hu et al., 2009). The nucleation mode and Aitken mode particles show a significant increase at midday on 28 January, while the accumulation mode is not significant. This may be ascribed to the emissions from vehicles and cooking near our sampling site. It is worth noting that the concentration of coarse-mode particles was highest on 28 and 29 January, which is consistent with the pattern of PM$_{2.5}$ / PM$_{10}$. After the coagulation, condensation and hygroscopic growth, the number concentrations of nucleation mode and Aitken mode particles decrease at 12:00 on 30 January, as shown in Fig. 6.

3.4 Aerosol chemical properties

The time series of chemical compositions, mass fractions, O : C ratio and m/z 44 of NR-PM$_1$ are presented in Fig. 7a–c. The average mass concentrations of organic, sulfate, nitrate, ammonium and chloride are 62.1 ± 46.1, 28.4 ± 22.1, 37.2 ± 30.6, 17.4 ± 12.7 and 5.5 ± 4.2 µg m^{-3}, respectively. The organic component is dominant in NR-PM$_1$, with an average mass fraction of 44.9 ± 11.7 %. Sulfate and nitrate species concentrations are also very high during the heavy-haze event.
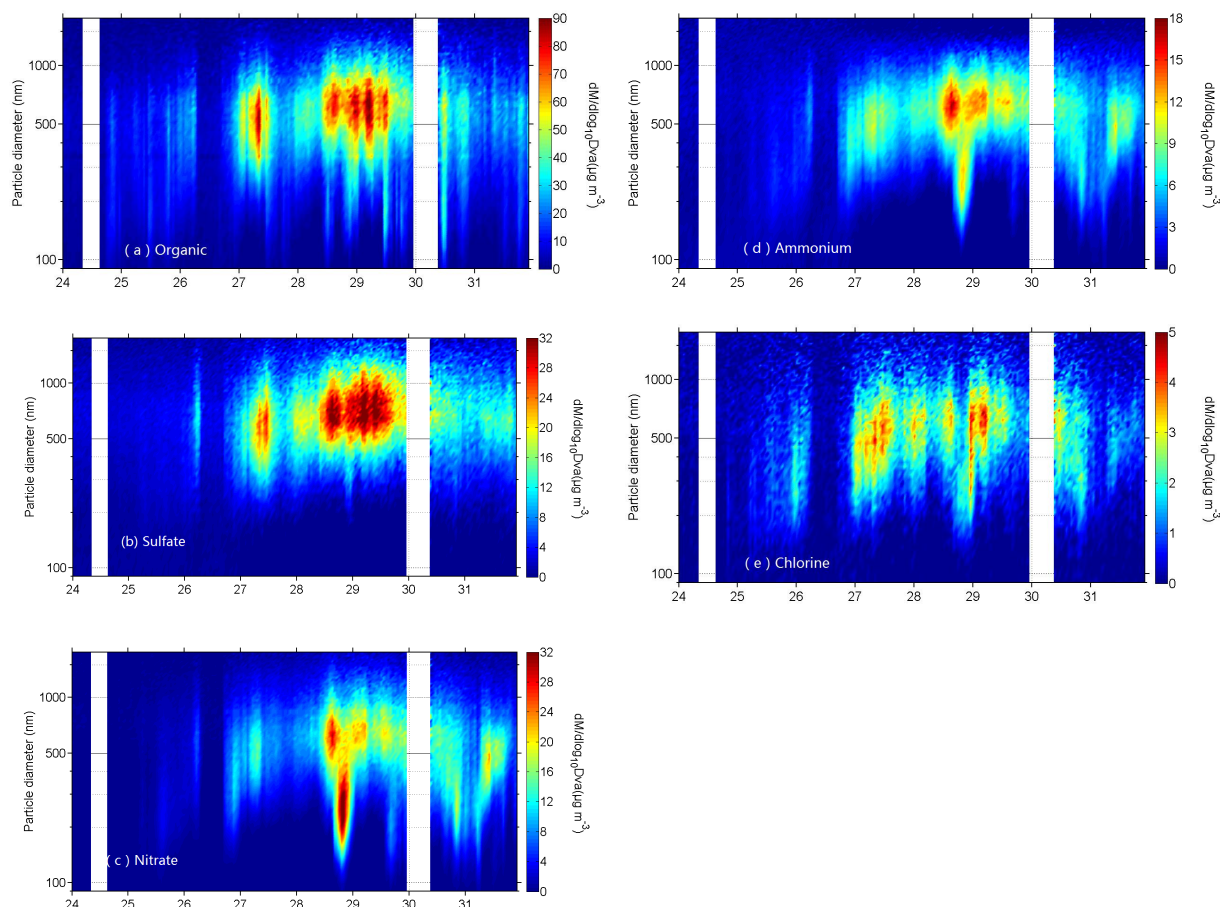
AMS enables the real-time determination of size-resolved chemical compositions of different modes of particles as a function of time. Figure 8 shows the temporal variations of the size distributions of the organic (a), sulfate (b), ni-
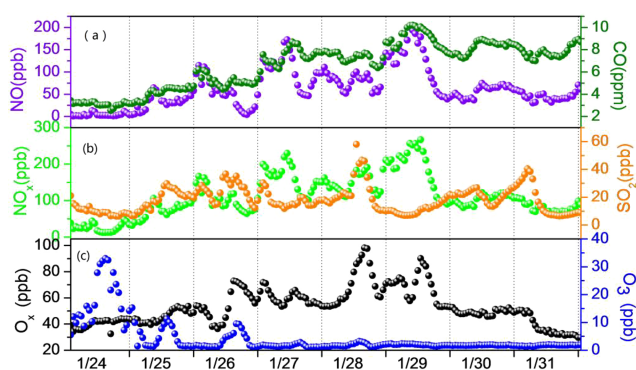
trate (c), ammonium (d) and chloride (e). The organic and chloride-containing particles display a slightly broader distribution than the other three species. All the aerosol components mainly reside in the accumulation mode with vacuum aerodynamic diameters around 700 nm. Note that the AMS size distributions here are shown as a function of vacuum aerodynamic diameter, D_{va}, which is the aerodynamic diameter measured under free-molecular regime flow conditions. To a first approximation, 700 nm in D_{va} corresponds roughly to 470 nm in physical diameter for spherical particles. It is worth noting that particles with optical diameters between 100 and 1000 nm have the highest scattering efficiency in the visible range (Liou, 2002), so a high concentration at this optimum aerosol size will lead to strong light scattering and reduced visibility during the period.

These five aerosol components all show high concentrations from the afternoon of 28 to noon on 29 January, corresponding with the highest mass loading and light scattering of the whole pollution period. The detailed behaviors of particle number concentration and size-resolved organic, sulfate, nitrate, ammonium and particle mass concentration on 28 January are presented in Figs. S5 and S6. The particle number concentrations show a burst at nearly 12:00, with D_m less than 100 nm. Observations by Sakurai et al. (2005) in Atlanta, GA, USA, recognized this as a plume related to a new particle formation event, which was accompanied by advection of local emissions. However, an increasing concentration of aerosol chemical components at about 11:00 on 28 January is observed by the AMS as shown in Fig. S5. The mass concentrations mainly reside on particles between 300 and 1000 nm in vacuum diameter. This may be due to the accumulation of air pollutants in the stagnant boundary layer. As we can see in Fig. S1, the meteorological parameters are characterized by calm wind, low RH and increasing temperature in the morning, which leads to a stable boundary layer. Then, with increasing surface temperature and PBL height,

Figure 8. Size-resolved chemical compositions of **(a)** organic, **(b)** sulfate, **(c)** nitrate, **(d)** ammonium and **(e)** chlorine.
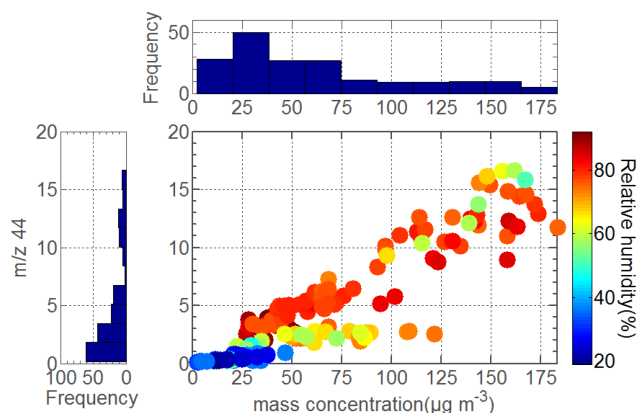

Figure 9. Mixing ratios of **(a)** NO and CO, **(b)** NO_x and SO_2, **(c)** O_x and O_3.

the dilution causes the aerosol concentration to decrease in the afternoon. The concentrations of sulfate, ammonium and nitrate show an increasing trend from 18:00. The major reasons are (1) that increasing RH may enhance the heterogeneous reaction of SO_2 and NH_3 to produce sulfate and nitrate; (2) that decreased PBL height at night leads to accumu-

lation of air pollutant; and (3) conversoin of N_2O_5 to nitrate via heterogonous or homogenous ways and reaction of OH and NO_2 (Kim et al., 2014). All of the above aspects result in the mass concentrations of nitrate and ammonium having a distinct growth of particles with diameters between 100 and 500 nm on 28 January.

3.5 Increased formation of secondary organic aerosol (SOA) during haze pollution episode

Figure 10 shows the variations of signal of m/z 44 as a function of organic aerosol mass concentration and the influence of relative humidity. The frequency distributions of organic mass and m/z 44 during the period are presented as well. The greatest frequency of occurrence of organic aerosol concentration appears nearly between mass concentrations of 20 and 35 µg m^{-3}, corresponding with a signal fraction of m/z 44 less than 2. The signal of m/z 44 shows an increasing trend with increasing organic mass. The lower concentration of the organic component mainly exists at RH below 40 %, which is indicative of a relatively clean atmosphere in urban Beijing. It is notable that the higher levels of the organic component occur under high-RH conditions, when aerosol water
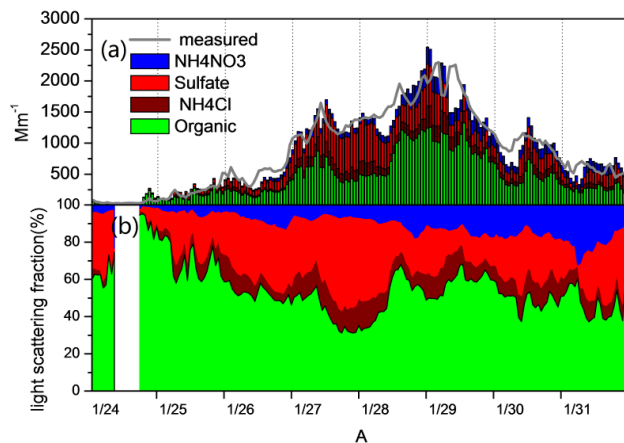
Figure 10. Lleft panel: the frequency distribution of m/z 44; top panel: the frequency distribution of organic mass; center panel: abundance of m/z 44 as a function of organic aerosol mass concentration and the influence of RH (left, color scale).

Figure 11. Time series of **(a)** apportioned light-scattering coefficients of each aerosol component compared with measured **(b)** light-scattering fractions of each aerosol components.

uptake ability is enhanced and the more highly hydrated particles are able to capture more water-soluble volatile organic compounds (VOCs). In this way, the dry mass concentration of organic aerosol increases after the water has evaporated in the AMS. The studies of Ge et al. (2012) in the Central Valley of California and Dall'Osto et al. (2009) in London also showed that aqueous-phase processes are responsible for the production of secondary organic aerosol species, most significantly during fog events.

3.6 Light-scattering apportionment

Light scattering by atmospheric aerosols is highly dependent on their size, morphology and compositions (Liou, 2002). Sulfate, nitrate, ammonium and organic components in aerosol contribute most to light scattering, particularly for diameters ranging from 100 to 1000 nm, which have the greatest light extinction efficiency (Seinfeld and Pandis, 1998). Here, a modified IMPROVE algorithm was employed to apportion light-scattering coefficients at $\lambda = 550$ nm (Pitchford et al., 2007). The IMPROVE algorithm was based on a multiple liner regression method (Chan et al., 1999), which considers the degree to which aerosol light scattering is related to the mass concentration of each component combined with water uptake of the inorganic component. The detailed introduction of the method can be found in Lowenthal et al. (1995). The f(RH) curve obtained by Chen et al. (2014) during January in the North China Plain is used here.

In our light apportionment calculation, the mass concentrations of ammonium sulfate, ammonium bisulfate, ammonium nitrate, ammonium chloride and organic were required. However, the AMS can only provide us with mass concentrations of sulfate, nitrate, ammonium chloride and organic compounds. Here, a commonly accepted ion pairing scheme of calculating the neutral aerosol from the molar number of all ions simplified by Gysel et al. (2007) is applied. In this
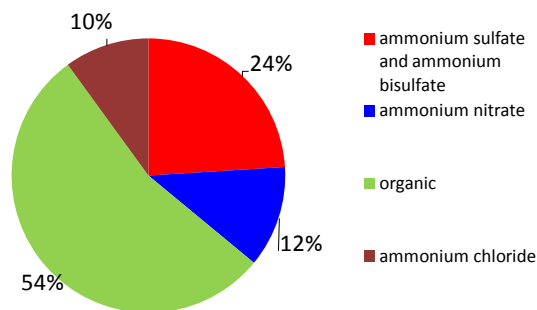
scheme, by setting the fraction of nitric acid to 0, the molar fraction of ammonium nitrate is equal to the molar fraction of nitrate ions. The rest of ammonium ions are assigned to ammonium bisulfate, ammonium sulfate and ammonium chloride according to ammonium molar fraction.

In the IMPROVE algorithm, the light-scattering growth due to inorganic components was considered, while the contribution from organic aerosol was not taken into account. Then, using the high-resolution mass concentrations of sulfate-containing aerosol, ammonium nitrate, ammonium chloride and organic in submicron aerosol and aerosol scattering growth curve, we calculated a relationship of scattering coefficient and aerosol components and light-scattering growth factor as shown in Eq. 9. The fitting was computed with MATLAB software (MATLAB R2010a). Figure 11a shows the time series of apportioned light-scattering coefficients of each of the aerosol components compared with measured values during the observation period. At the beginning of the periods, organic components dominated light scattering. With the development of the haze, the contribution of inorganic components increased as shown in Fig. 11b. The total average light-scattering contribution of each aerosol component is presented in Fig. 12. The apportionment contributions from organic, sulfate, ammonium nitrate and ammonium chloride were 54, 24, 12 and 10 %, respectively, which indicated the dominant contribution of organic and sulfate compounds to light scattering during this haze episode in Beijing. One should note that the apportioned light-scattering coefficient using the IMPROVE method is highly related to its mass concentration, and organic aerosol is a large fraction of the mass. Yao et al. (2010) showed that the organic components contributed greatly to the light extinction (about 45 % contribution) by using AMS data during winter in Shenzhen, PRC. Watson (2002) also found that organic aerosol dominated light extinction in some cities, with

Figure 12. Averaged light-scattering contribution of each aerosol component during the haze episode.

fractions of 9–50 % in the eastern USA.

$$\sigma_{sp}^{550} = 6.5\,f\,(\text{RH})[(\text{NH}_4)_2\text{SO}_4] + 6.5\,f\,(\text{RH})[\text{NH}_4\text{HSO}_4]$$
$$+ 2.2\,f\,(\text{RH})[\text{NH}_4\text{NO}_3]$$
$$+ 4.3\,f\,(\text{RH})[\text{NH}_4\text{Cl}] + 5.7[\text{organic}] + 57.3 \quad (5)$$

4   Summary and conclusion

Based on in situ measurements, the physical and chemical properties of aerosol particles were characterized during a severe haze episode in Beijing from 24 to 31 January 2013. The average mass concentrations of PM_1, $PM_{2.5}$ and PM_{10} were 99.1 ± 67.1, 188.3 ± 128.8 and $265.2 \pm 157.1\,\mu g\,m^{-3}$, respectively, and an increasing fraction of $PM_{1-2.5}$ was significant during the heaviest pollution periods. The averaged scattering coefficient at 550 nm was $877.2 \pm 624.2\,\text{Mm}^{-1}$, and an increasing amount of relatively coarse particles also can be seen from the variations of backscattering ratios, asymmetry parameter and scattering Ångström exponent. Particle number-size distribution (14 to 2500 nm) showed high number concentrations in the nucleation and accumulation modes. Size-resolved chemical composition of submicron aerosol from a HR-ToF-AMS showed that the mass concentration of organic, sulfate, nitrate, ammonium and chlorine mainly resided on particles 500–800 nm in vacuum diameter, and sulfate and ammonium contributed to the growth of particles during the most heavily polluted day on 28 January.

High emissions of regional background pollutants combined with stable synoptic conditions and increasing relative humidity, which lead to enhanced water uptake ability of submicron aerosol and formation of secondary aerosol, may be the main reasons for the heavy-haze episode. Light-scattering apportionment showed that organic, sulfate-containing components, ammonium nitrate and ammonium chloride contributed to light-scattering fractions of 54, 24, 12 and 10 %, respectively. Considering their dominant fractional contribution to light scattering and light extinction, our study indicated that organic components also played an important role

in visibility degradation during the winter haze episode in Beijing.

The Supplement related to this article is available online at doi:10.5194/acp-15-3205-2015-supplement.

References

Anderson, T. L. and Ogren, J. A.: Determining Aerosol Radiative Properties Using the Tsi 3563 Integrating Nephelometer, Aerosol. Sci. Tech., 29, 57–69, doi:10.1080/02786829808965551, 1998.

Anderson, T. L., Charlson, R. J., Schwartz, S. E., Knutti, R., Boucher, O., Rodhe, H., and Heintzenberg, J.: Atmospheric science. Climate forcing by aerosol – a hazy picture, Science, 300, 1103–1104, 2003.

Andrews, E., Sheridan, P. J., Fiebig, M., McComiskey, A., Ogren, J. A., Arnott, P., Covert, D., Elleman, R., Gasparini, R., Collins, D., Jonsson, H., Schmid, B., and Wang, J.: Comparison of methods for deriving aerosol asymmetry parameter, J. Geophys. Res., 111, D05S04, doi:10.1029/2004JD005734, 2006.

Beddows, D. C. S., Dall'osto, M., and Harrison, R. M.: An Enhanced Procedure for the Merging of Atmospheric Particle Size Distribution Data Measured Using Electrical Mobility and Time-of-Flight Analysers, Aerosol. Sci. Tech., 44, 930–938, 2010.

Chan, Y. C., Simpson, R. W., McTainsh, G. H., Vowles, P. D., Cohen, D. D., and Bailey, G. M.: Source apportionment of visibility degradation problems in Brisbane (Australia) using the multiple linear regression techniques, Atmos. Environ., 33, 3237–3250, 1999.

Chen, J., Zhao, C. S., Ma, N., Liu, P. F., Göbel, T., Hallbauer, E., Deng, Z. Z., Ran, L., Xu, W. Y., Liang, Z., Liu, H. J., Yan, P., Zhou, X. J., and Wiedensohler, A.: A parameterization of low visibilities for hazy days in the North China Plain, Atmos. Chem. Phys., 12, 4935–4950, doi:10.5194/acp-12-4935-2012, 2012.

Chen, J., Zhao, C. S., Ma, N., and Yan, P.: Aerosol hygroscopicity parameter derived from the light scattering enhancement factor measurements in the North China Plain, Atmos. Chem. Phys., 14, 8105–8118, doi:10.5194/acp-14-8105-2014, 2014.

Cheng, Y. F., Su, H., Rose, D., Gunthe, S. S., Berghof, M., Wehner, B., Achtert, P., Nowak, A., Takegawa, N., Kondo, Y., Shiraiwa, M., Gong, Y. G., Shao, M., Hu, M., Zhu, T., Zhang, Y. H., Carmichael, G. R., Wiedensohler, A., Andreae, M. O., and Pöschl, U.: Size-resolved measurement of the mixing state

of soot in the megacity Beijing, China: diurnal cycle, aging and parameterization, Atmos. Chem. Phys., 12, 4477–4491, doi:10.5194/acp-12-4477-2012, 2012.

Dall'Osto, M., Harrison, R. M., Coe, H., and Williams, P.: Real-time secondary aerosol formation during a fog event in London, Atmos. Chem. Phys., 9, 2459–2469, doi:10.5194/acp-9-2459-2009, 2009.

Deng, Z. Z., Zhao, C. S., Ma, N., Ran, L., Zhou, G. Q., Lu, D. R., and Zhou, X. J.: An examination of parameterizations for the CCN number concentration based on in situ measurements of aerosol activation properties in the North China Plain, Atmos. Chem. Phys., 13, 6227–6237, doi:10.5194/acp-13-6227-2013, 2013.

Garland, R. M., Yang, H., Schmid, O., Rose, D., Nowak, A., Achtert, P., Wiedensohler, A., Takegawa, N., Kita, K., Miyazaki, Y., Kondo, Y., Hu, M., Shao, M., Zeng, L. M., Zhang, Y. H., Andreae, M. O., and Pöschl, U.: Aerosol optical properties in a rural environment near the mega-city Guangzhou, China: implications for regional air pollution, radiative forcing and remote sensing, Atmos. Chem. Phys., 8, 5161–5186, doi:10.5194/acp-8-5161-2008, 2008.

Ge, X., Zhang, Q., Sun, Y., Ruehl, C. R., and Setyan, A.: Effect of aqueous-phase processing on aerosol chemistry and size distributions in Fresno, California, during wintertime, Environ. Chem., 9, 221–235, 2012.

Gysel, M., Crosier, J., Topping, D. O., Whitehead, J. D., Bower, K. N., Cubison, M. J., Williams, P. I., Flynn, M. J., McFiggans, G. B., and Coe, H.: Closure study between chemical composition and hygroscopic growth of aerosol particles during TORCH2, Atmos. Chem. Phys., 7, 6131–6144, doi:10.5194/acp-7-6131-2007, 2007.

He, X., Li, C. C., Lau, A. K. H., Deng, Z. Z., Mao, J. T., Wang, M. H., and Liu, X. Y.: An intensive study of aerosol optical properties in Beijing urban area, Atmos. Chem. Phys., 9, 8903–8915, doi:10.5194/acp-9-8903-2009, 2009.

Hu, M., He, L., Huang, X., and Wu, Z.: Chmeical and physical properties, source and formation of fine and ultrafine particle in Beijing, Science Press, 163–171, 2009.

Huang, K., Zhuang, G., Lin, Y., Li, J., Sun, Y., Zhang, W., and Fu, J. S.: Relation between optical and chemical properties of dust aerosol over Beijing, China, J. Geophys. Res., 115, D00K16, 2010a.

Huang, X.-F., He, L.-Y., Hu, M., Canagaratna, M. R., Sun, Y., Zhang, Q., Zhu, T., Xue, L., Zeng, L.-W., Liu, X.-G., Zhang, Y.-H., Jayne, J. T., Ng, N. L., and Worsnop, D. R.: Highly time-resolved chemical characterization of atmospheric submicron particles during 2008 Beijing Olympic Games using an Aerodyne High-Resolution Aerosol Mass Spectrometer, Atmos. Chem. Phys., 10, 8933–8945, doi:10.5194/acp-10-8933-2010, 2010b.

Kaufman, Y. J., Koren, I., Remer, L. A., Rosenfeld, D., and Rudich, Y.: The effect of smoke, dust, and pollution aerosol on shallow cloud development over the Atlantic Ocean, P. Natl. Acad. Sci. USA, 102, 11207–11212, 2005.

Kim, Y. J., Spak, S. N., Carmichael, G. R., Riemer, N., and Stanier, C. O.: Modeled aerosol nitrate formation pathways during wintertime in the Great Lakes region of North America, J. Geophys. Res.-Atmos., 119, 12420–12445, doi:10.1002/2014JD022320, 2014.

Koren, I., Kaufman, Y. J., Rosenfeld, D., Remer, L. A., and Rudich, Y.: Aerosol invigoration and restructuring of Atlantic convective clouds, Geophys. Res. Lett., 32, L14828, 2005.

Li, W. J., Shao, L. Y., and Buseck, P. R.: Haze types in Beijing and the influence of agricultural biomass burning, Atmos. Chem. Phys., 10, 8119–8130, doi:10.5194/acp-10-8119-2010, 2010.

Liou, K. N.: An introduction to atmospheric radiation (2nd Edition), Elsevier Science, 2002.

Liu, X. G., Li, J., Qu, Y., Han, T., Hou, L., Gu, J., Chen, C., Yang, Y., Liu, X., Yang, T., Zhang, Y., Tian, H., and Hu, M.: Formation and evolution mechanism of regional haze: a case study in the megacity Beijing, China, Atmos. Chem. Phys., 13, 4501–4514, doi:10.5194/acp-13-4501-2013, 2013.

Liu, Z., Hu, B., Wang, L., Wu, F., Gao, W., and Y. Wang: Seasonal and diurnal variation in particulate matter (PM_{10} and $PM_{2.5}$) at an urban site of Beijing: analyses from a 9-year study, Environ. Sci. Pollut. R., 22, 627–642, 2015.

Liu, Z. R., Hu, B., Liu, Q., Sun, Y., and Wang, Y. S.: Source apportionment of urban fine particle number concentration during summertime in Beijing, Atmos. Environ, 96, 359–369, 2014.

Lohmann, U. and Feichter, J.: Global indirect aerosol effects: a review, Atmos. Chem. Phys., 5, 715–737, doi:10.5194/acp-5-715-2005, 2005.

Lowenthal, D. H., Rogers, C. F., Saxena, P., Watson, J. G., and Chow, J. C.: Sensitivity of estimated light extinction coefficients to model assumptions and measurement errors, Atmos. Environ., 29, 751–766, 1995.

Ma, N., Zhao, C. S., Müller, T., Cheng, Y. F., Liu, P. F., Deng, Z. Z., Xu, W. Y., Ran, L., Nekat, B., van Pinxteren, D., Gnauk, T., Müller, K., Herrmann, H., Yan, P., Zhou, X. J., and Wiedensohler, A.: A new method to determine the mixing state of light absorbing carbonaceous using the measured aerosol optical properties and number size distributions, Atmos. Chem. Phys., 12, 2381–2397, doi:10.5194/acp-12-2381-2012, 2012.

Meier, J., Wehner, B., Massling, A., Birmili, W., Nowak, A., Gnauk, T., Brüggemann, E., Herrmann, H., Min, H., and Wiedensohler, A.: Hygroscopic growth of urban aerosol particles in Beijing (China) during wintertime: a comparison of three experimental methods, Atmos. Chem. Phys., 9, 6865–6880, doi:10.5194/acp-9-6865-2009, 2009.

Nel, A.: Atmosphere. Air pollution-related illness: effects of particles, Science, 308, 804–806, 2005.

Pan, X. L., Yan, P., Tang, J., Ma, J. Z., Wang, Z. F., Gbaguidi, A., and Sun, Y. L.: Observational study of influence of aerosol hygroscopic growth on scattering coefficient over rural area near Beijing mega-city, Atmos. Chem. Phys., 9, 7519–7530, doi:10.5194/acp-9-7519-2009, 2009.

Pitchford, M., Malm, W., Schichtel, B., Kumar, N., Lowenthal, D., and Hand, J.: Revised Algorithm for Estimating Light Extinction from IMPROVE Particle Speciation Data, JAPCA J. Air Waste Ma., 57, 1326–1336, 2007.

Pöschl, U.: Atmospheric aerosols: composition, transformation, climate and health effects, Angew. Chem. Int. Ed. Engl., 44, 7520–7540, 2005.

Qu, W. J., Arimoto, R., Zhang, X. Y., Zhao, C. H., Wang, Y. Q., Sheng, L. F., and Fu, G.: Spatial distribution and interannual variation of surface PM_{10} concentrations over eighty-six Chinese cities, Atmos. Chem. Phys., 10, 5641–5662, doi:10.5194/acp-10-5641-2010, 2010.

Quan, J., Zhang, Q., He, H., Liu, J., Huang, M., and Jin, H.: Analysis of the formation of fog and haze in North China Plain (NCP), Atmos. Chem. Phys., 11, 8205–8214, doi:10.5194/acp-11-8205-2011, 2011.

Ramanathan, V., Crutzen, P. J., Kiehl, J. T., and Rosenfeld, D.: Aerosols, climate, and the hydrological cycle, Science, 294, 2119–2124, 2001.

Sakurai, H., Fink, M. A., McMurry, P. H., Mauldin, L., Moore, K. F., Smith, J. N., and Eisele, F. L.: Hygroscopicity and volatility of 4–10 nm particles during summertime atmospheric nucleation events in urban Atlanta, J. Geophys. Res.-Atmos., 110, D22S04, 2005.

Seinfeld, J. H. and Pandis, S. N.: Atmospheric Chemistry and physics, From Air Pollution to Climate Changes, Wiley, New York, USA, 1998.

Shi, J. P., Evans, D. E., Khan, A. A., and Harrison, R. M.: Sources and concentration of nanoparticles (< 10 nm diameter) in the urban atmosphere, Atmos. Environ., 35, 1193–1202, 2001.

Sun, Y. L., Zhuang, G. S., Tang, A., Wang, Y., and An, Z.: Chemical Characteristics of $PM_{2.5}$ and PM_{10} in Haze-fog Episodes in Beijing, Environ. Sci. Technol., 40, 3148–3155, 2006.

Tang, G., Wang, Y., Li, X., Ji, D., Hsu, S., and Gao, X.: Spatial-temporal variations in surface ozone in Northern China as observed during 2009–2010 and possible implications for future air quality control strategies, Atmos. Chem. Phys., 12, 2757–2776, doi:10.5194/acp-12-2757-2012, 2012.

Titos, G., Foyo-Moreno, I., Lyamani, H., Querol, X., Alastuey, A., and Alados-Arboledas, L.: Optical properties and chemical composition of aerosol particles at an urban location: An estimation of the aerosol mass scattering and absorption efficiencies, J. Geophys. Res.-Atmos., 117, D04206, doi:10.1029/2011jd016671, 2012.

Twomey, S.: The Influence of Pollution on the Shortwave Albedo of Clouds, J. Atmos. Sci., 34, 1149–1152, 1977.

Wang, K. C., Dickinson, R. E., Su, L., and Trenberth, K. E.: Contrasting trends of mass and optical properties of aerosols over the Northern Hemisphere from 1992 to 2011, Atmos. Chem. Phys., 12, 9387–9398, doi:10.5194/acp-12-9387-2012, 2012.

Wang, L., Xu, J., Yang, J., Zhao, X., Wei, W., Cheng, D., Pan, X., and Su, J.: Understanding haze pollution over the southern Hebei area of China using the CMAQ model, Atmos. Environ., 56, 69–79, 2012.

Wang, Y., Yao, L., Wang, L., Liu, Z., Ji, D., Tang, G., Zhang, J., Sun, Y., Hu, B., and Xin, J.: Mechanism for the formation of the January 2013 heavy haze pollution episode over central and eastern China, Science China Earth Sciences, 57, 14–25, 2013.

Wang, Y. H., Hu, B., Ji, D. S., Liu, Z. R., Tang, G. Q., Xin, J. Y., Zhang, H. X., Song, T., Wang, L. L., Gao, W. K., Wang, X. K., and Wang, Y. S.: Ozone weekend effects in the Beijing–Tianjin–Hebei metropolitan area, China, Atmos. Chem. Phys., 14, 2419–2429, doi:10.5194/acp-14-2419-2014, 2014.

Watson, J. G.: Visibility: Science and Regulation, JAPCA J. Air Waste Ma., 52, 628–713, 2002.

Wehner, B., Birmili, W., Ditas, F., Wu, Z., Hu, M., Liu, X., Mao, J., Sugimoto, N., and Wiedensohler, A.: Relationships between submicrometer particulate air pollution and air mass history in Beijing, China, 2004–2006, Atmos. Chem. Phys., 8, 6155–6168, doi:10.5194/acp-8-6155-2008, 2008.

Willeke, K. and Baron, P. A.: Aerosol Measurement Principles, Techniques, and Applications, Van Nostrand Reinhold, Hoboken, NJ, USA, 1993.

Wu, Z., Hu, M., Liu, S., Wehner, B., Bauer, S., Maßling, A.: New particle formation in Beijing, China: Statistical analysis of a 1-year data set, J. Geophys. Res., 112, D09209, doi:10.1029/2006jd007406, 2007.

Yang, M., Howell, S. G., Zhuang, J., and Huebert, B. J.: Attribution of aerosol light absorption to black carbon, brown carbon, and dust in China – interpretations of atmospheric measurements during EAST-AIRE, Atmos. Chem. Phys., 9, 2035–2050, doi:10.5194/acp-9-2035-2009, 2009.

Yao, T., Huang, X., He, L., Hu, M., Sun, T., Xue, L., Lin, Y., Zeng, L., and Zhang, Y.: High time resolution observation and statistical analysis of atmospheric light extinction properties and the chemical speciation of fine particulates, Science China Chemistry, 53, 1801–1808, 2010.

Zhang, J. K., Sun, Y., Liu, Z. R., Ji, D. S., Hu, B., Liu, Q., and Wang, Y. S.: Characterization of submicron aerosols during a month of serious pollution in Beijing, 2013, Atmos. Chem. Phys., 14, 2887–2903, doi:10.5194/acp-14-2887-2014, 2014.

Zhang, Q., Stanier, C. O., Canagaratna, M. R., Jayne, J. T., Worsnop, D. R., Pandis, S. N., and Jimenez, J. L.: Insights into the Chemistry of New Particle Formation and Growth Events in Pittsburgh Based on Aerosol Mass Spectrometry, Environ. Sci. Technol., 38, 4797–4809, 2004.

Zhang, Q., Quan, J., Tie, X., Huang, M., and Ma, X.: Impact of aerosol particles on cloud formation: Aircraft measurements in China, Atmos. Environ., 45, 665–672, 2011.

Zhang, Q. H., Zhang, J. P., and Xue, H. W.: The challenge of improving visibility in Beijing, Atmos. Chem. Phys., 10, 7821–7827, doi:10.5194/acp-10-7821-2010, 2010.

Zhang, X., Sun, J., Wang, Y., Li, W., Zhang, Q., Wang, W., Quan, J., Cao, G., Wang, J., Yang, Y., and Zhang, Y.: Factors contributing to haze and fog in China, Chinese Sci. Bull. (Chinese Version), 58, 1178–1187, 2013.

Zhang, X. Y., Wang, Y. Q., Niu, T., Zhang, X. C., Gong, S. L., Zhang, Y. M., and Sun, J. Y.: Atmospheric aerosol compositions in China: spatial/temporal variability, chemical signature, regional haze distribution and comparisons with global aerosols, Atmos. Chem. Phys., 12, 779–799, doi:10.5194/acp-12-779-2012, 2012.

Zhao, X. J., Zhao, P. S., Xu, J., Meng, W., Pu, W. W., Dong, F., He, D., and Shi, Q. F.: Analysis of a winter regional haze event and its formation mechanism in the North China Plain, Atmos. Chem. Phys., 13, 5685–5696, doi:10.5194/acp-13-5685-2013, 2013.